Journal of Thermal Science Vol.32, No.3 (2023) 1239−1250

https://doi.org/10.1007/s11630-023-1786-y **Article ID: 1003-2169(2023)03-1239-12**

A New Structure of Cooling Wall Tube for Supercritical CO_2 Coal-Fired Power Plants

WANG Yanjuan[1], GAO Shuo[1], JIANG Qiongqiong[1*], LI Yi[1], LIU Qibin[2,3], XU Jinliang[1]

1. The Beijing Key Laboratory of Multiphase Flow and Heat Transfer, North China Electric Power University, Beijing 102206, China
2. Institute of Engineering Thermophysics, Chinese Academy of Sciences, Beijing 100190, China
3. University of Chinese Academy of Sciences, Beijing 100049, China

Abstract: In terms of developing supercritical CO_2 (sCO_2) coal-fired power plants, enhancing cooling wall performance is one of significant factors to improve system performance. In this paper, a new cooling wall tube structure is proposed to match the non-uniform heat flux (NUH) with the thermal resistance by changing the cooling wall tube eccentricity. A three-dimensional multi-physical coupling model of cooling wall is constructed to compare the novel structure to the conventional structures. The properties of fluid dynamics, thermal stress, coupled heat transfer and cooling wall deformation are analyzed. In contrast to the traditional structure, the maximum temperature and circumferential temperature difference (CTD) of the proposed structure can be reduced by 2% and 27.4%, respectively. The essential working parameters related to the performances of the cooling wall tube are discussed. The maximum temperature of the new structure is reduced by 8–13 K and the maximum thermal stress is reduced by about 10%–15% under all the simulated working conditions when the eccentricity changes from 0 to 0.2. The proposed structure can effectively reduce the maximum temperature and circumferential temperature gradient under NUH. Consequently, a novel insight is put out for the design and optimization of the cooling wall tube in coal-fired power plants.

Keywords: supercritical carbon dioxide, cooling wall tube, thermal-hydraulic-structural coupling, supercritical heat transfer

1. Introduction

As the proportion of renewable energy consumption in the world is gradually increasing, the modern electric grid operates in the form of multi-energy complementation. The modern electric grid should respond fast to load variations [1] due to renewable energies' unstable and variable characteristics. However, traditional fossil-energy-driven power plants with water-steam Rankine cycle operate slowly for peak load regulation [2]. Supercritical carbon dioxide (sCO_2) is considered a promising alternative heat transfer fluid for fossil-energy-driven power plants owing to the advantages of high efficiency, chemically inactive, and higher compactness [3]. The compactness of the sCO_2 cycle enables more flexible peak load regulation of

Received: Nov 20, 2022
AE: LI Mingjia
Corresponding author: JIANG Qiongqiong E-mail: 90102607@ncepu.edu.cn

Nomenclature

CTD	circumferential temperature difference/K	δ_m	minimum thickness/mm
C_p	specific heat/J·kg^{-1}·K^{-1}	λ	thermal conductivity/W·m^{-1}·K^{-1}
D	tube outer diameter/mm	ξ	allowable stress correction factor
d	tube inner diameter/mm	ρ	density/kg·m^{-3}
E	elastic modulus/MPa	σ_{as}	maximum allowable stress/MPa
E_c	eccentricity	σ_{eq}	equivalent stress/MPa
e	eccentric distance/mm	$\sigma_{t,max}$	maximum cross-sectional thermal stress/MPa
G	mass flux/kg·s^{-1}·m^{-2}	υ	Poisson's ratio
i	enthalpy/kJ·kg^{-1}	φ	view factor
L	tube length/m	**Subscripts**	
NUH	non-uniform heat flux	ave	average
P	working pressure/MPa	b,i	inner wall at bottom generatrix
ΔP	pressure drop/kPa	b,o	outer wall at bottom generatrix
q	heat flux/kW·m^{-2}	bs	backfire side
R	tube outer radius/mm	f	fluid
r	tube inner radius/mm	fs	fireside
S	tube pitch/mm	in	inlet of tube
T	temperature/K	r, θ, l	radial, tangential and axial direction
ΔT	temperature difference/K	t,i	inner wall at top generatrix
UH	uniform heat flux	t,o	outer wall at top generatrix
Y	correction coefficient	w	tube wall
Greek symbols		w,i	inner wall of tube
α	circumferential angle/(°) or thermal expansion coefficient/K^{-1}	w,o	outer wall of tube
α_{max}	limiting angle/(°)		

power plants [4], which provides a new solution to the "wind and light abandonment" caused by the grid connection of renewable energy.

More attention has been drawn to sCO_2 fossil-fired power plants in recent years [5, 6]. In 2013, Le Moullec [7] developed the conceptual design of a sCO_2 fossil-fired power plant. Maxson et al. [8] and Xu [9] made a thermodynamic and economic study of sCO_2 coal-fired power plants, demonstrating its better performances. Li et al. [10] developed an integrated model combining the sCO_2 Brayton cycle with printed circuit heat exchanger and proposed a new criterion to evaluate the performance of the recuperator in sCO_2 Brayton cycle. Fan et al. [11] made a review on recent advances and development of sCO_2 power systems. A 5 MW sCO_2 integral test facility was constructed to study the key equipment and cycle thermodynamic performances by Xi'an Thermal Power Research Institute [12].

The sCO_2 boiler is a vital part of the sCO_2 power plants, in which the structure design of cooling walls is usually based on a detailed study of the thermal and hydraulic features of sCO_2 in cooling wall tubes. Much work has been done by Xu et al. [13, 14] to solve key issues of the sCO_2 boiler, the problems associated with large pressure drop (ΔP), and energy extraction from residual flue gas. Yang et al. [12] developed a one-dimensional model to study the heat transfer processes of the cooling wall, superheater, and reheater in a 20 MW sCO_2 boiler, and the results indicated that the maximum tube wall temperature of 907 K appears at the outlet region of the front wall. Zhou et al. [15] constructed a one-dimensional thermal-fluid model of sCO_2 cooling walls, and discussed the effects of flow direction and tube diameter on tube temperature difference. Wang et al. [16] studied the thermal performances of sCO_2 tubes, and concluded that the inclined angle had little effects on the heat transfer coefficient.

The safety of cooling walls in sCO_2 boiler is a challenging problem [17]. Compared with the traditional water walls, the convective heat transfer coefficient of sCO_2 is lower [18] and the working temperature is higher [19]. Various strategies have been developed in recent years to decrease cooling wall temperatures and the non-uniformity of cooling walls' circumferential temperature. Zhou et al. [20] proposed partial expansion at the upper

zone of the boiler size and double furnace, and the new structure can reduce the average heat duty by about 50%. Liu et al. [21] improved the coupling between heat flux and cooling wall tubes in both the width and height directions of the furnace. sCO_2 flow rate redistributes by restriction orifices to adapt to the NUH in the furnace width direction, decreasing cooling wall temperature by about 13 K. In the furnace height direction, flow direction was changed at the peak heat flux point to match the heat flux variations, and thus, the cooling wall temperature can be reduced by about 4.4 K. Additionally, many heat transfer enhancement structures have been proposed. Muñoz and Abánades [22] presented a typical method using internal spiral finned tubes in a parabolic slot collector. This design reduced the maximum temperature of the tube wall, while the pressure drop shows a certain degree of increase. Li et al. [23] utilized the internal twisted tapes and arranged unilateral elliptic dimples inside the tube to reduce the circumferential temperature gradient. The circumferential temperature gradient was significantly reduced. However, a twisted tape insertion tube substantially increases pressure drop, and the unilateral elliptical recessed tube leads to certain flow resistance and stress concentration.

Unlike existing methods, by matching the external heat flux density distribution with the thermal resistance of the cooling wall tube, a novel structure is developed to boost the performance of the cooling wall tube in this study. This proposed structure is simpler and more flexible. A model of thermal-hydraulic-structural coupling is created to analyze the new structure's performance. The novelties and contributions lie in the following items:

(1) A three-dimensional multi-physical coupling model, including energy, fluid flow, mass conservation governing equations, and static structure calculation, is proposed to analyze the performances of the cooling wall tubes in sCO_2 boiler. The distributions of temperature, stress intensity, and deformation of the cooling wall tube are numerically acquired.

(2) A new cooling wall tube structure is proposed to improve the thermal-structural performance via changing the eccentricity, which makes the heat flux level match its thermal resistance. A comparison study between the traditional and new structures is made. Furthermore, the critical operating parameters affecting heat transfer performance are discussed.

2. Numerical Model and Method

2.1. The sCO_2 cooling wall tube model

The heat transfer of the cooling wall is complex as the heat flux changes along the furnace's width, depth, and height directions. In the circumferential direction, since the heat flux on the rear surface (the side close to the boiler wall) of the cooling wall tubes is very small, their rear parts are almost unheated. While these tubes were exposed to the boiler furnace on the fireside, the heat flux became much high. In addition, the density of the heat flux changes with the distance from the burner in the flow direction.

In this paper, we investigated the cooling wall made of bare tubes, and the schematic diagram of sCO_2 cooling wall tubes is shown in Fig. 1. As shown in Fig. 1(a), the smooth cooling wall tube is a seamless steel tube, which is arranged in parallel close to the inner wall of the furnace, and the pitch distance (S) is 55.5 mm. The inlet and outlet ends are connected to the lower and upper headers, respectively. A vertical circular tube made of T91 with outer diameter (D) 35 mm and inner diameter (d) 22 mm is adopted, as presented in Fig. 1(b). A unit

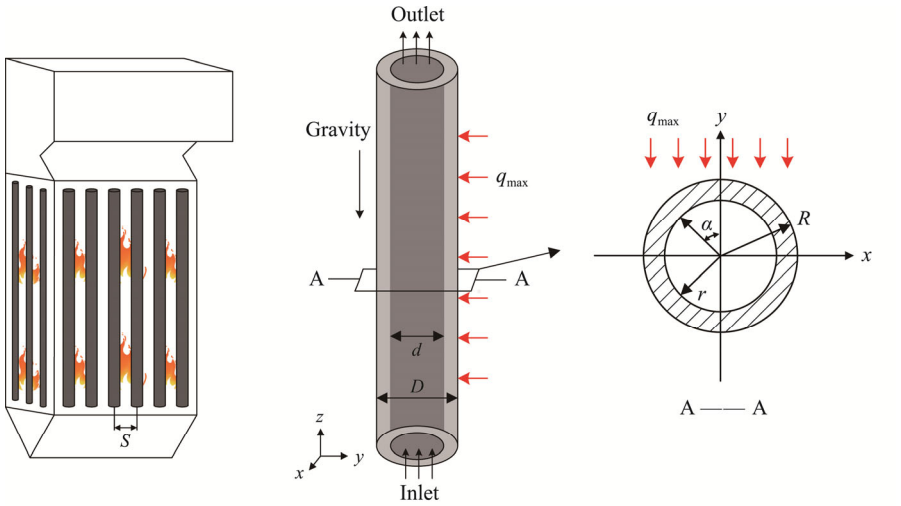

(a) Arrangement in boiler (b) Physical configuration (c) Detailed circumferential information

Fig. 1 Schematic diagram of cooling wall of sCO_2 boiler

length of 1 m was taken for the cooling wall tube to facilitate modeling and simplify calculations. The gravity is contrary to the sCO_2 flow direction. The outer tube wall adopts the NUH boundary condition. Fig. 1(c) shows the specific section circumferential information. The circumferential angle (α) on the top generatrix is defined as 0°.

2.2 Non-uniform heat flux distribution

One of the key issues in the three-dimensional numerical simulation of sCO_2 boiler cooling walls is to obtain high-quality external heat flux distribution. The study of a 600 MW supercritical boiler from Ref. [14] demonstrated that the cooling wall tubes in the furnace are mainly heated by the flame radiation while the fraction of the convection heat transfer only contributes around 5.5%. Thus, only radiative heat transfer is considered in this modeling. According to Refs. [24, 25], the view factor (φ) is defined to describe the circumferential non-uniform radiant heat flux distribution of the cooling wall tube. The cross-section irradiation profile of the sCO_2 cooling wall tube is shown in Fig. 2, where R is the tube's outer radius, and α is its circumferential angle.

The view factor is defined as:

$$\varphi = \frac{q_\alpha}{q_{\max}} \tag{1}$$

where $q_{\max}$ is the external effective radiant maximum heat flux, and q_α is the heat flux at a specific angle around the outer wall of the cooling wall tube. q_α is composed of two parts: the fireside radiation heat flux (q_{fs}) and the reflected heat flux from the backfire side (q_{bs}). Their relationship is expressed to:

$$K = \frac{q_{\text{bs}}}{q_{\text{fs}}} = \frac{\sqrt{c^2-1} - \operatorname{arctg}\sqrt{c^2-1}}{c} \tag{2}$$

where c=S/2R.

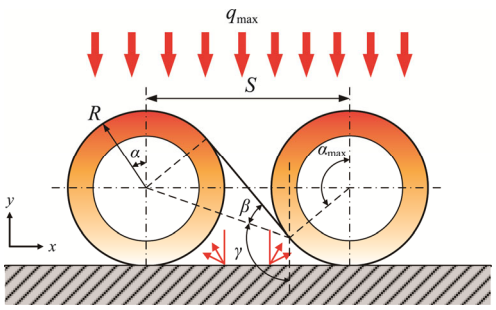

Fig. 2 Cross-section irradiation profile of the sCO_2 cooling wall tube

Similarly, the view factor consists of the fireside view factor (φ_{fs}) and the backfire side view factor (φ_{bs}), and the relationship is

$$\varphi = \varphi_{\text{fs}} + K\varphi_{\text{bs}} \tag{3}$$

According to Ref. [24], the distributions of φ_{fs} and φ_{bs} on the outer surface of the cooling wall tube are obtained, respectively. Then, the distribution of φ can be obtained as follows:

$$\varphi = \frac{1}{2}\left[1+\sin\left(\alpha+\beta+\gamma\right)\right], 0 \le \alpha \le \pi - \alpha_{\max} \tag{4}$$

$$\varphi = \frac{1}{2}\left[1+\sin\left(\alpha+\beta+\gamma\right)\right] + \frac{1}{2}K\left[1+\sin\left(\beta-\gamma-\alpha\right)\right], \quad \pi - \alpha_{\max} \le \alpha \le \frac{\pi}{2} \tag{5}$$

$$\varphi = \frac{1}{2}\left[1+\sin\left(\alpha+\beta+\pi-\gamma\right)\right] + \frac{1}{2}\mathrm{K}\left[1+\sin\left(\pi-\alpha+\beta+\gamma\right)\right], \frac{\pi}{2} \le \alpha < \alpha_{\max} \tag{6}$$

$$\varphi = \frac{1}{2}K\left[1+\sin\left(\pi-\alpha+\beta+\gamma\right)\right], \alpha_{\max} \le \alpha \le \pi \tag{7}$$

The limiting angle $\alpha_{\max}$, β, γ are, respectively, calculated by

$$\alpha_{\max} = \arccos\left(\frac{2R}{S}\right) + \frac{\pi}{2} \tag{8}$$

$$\beta = \arcsin\left[\frac{R}{\sqrt{(S-R\sin\alpha)^2 + (R\cos\alpha)^2}}\right] \tag{9}$$

$$\gamma = \arcsin\left[\frac{S-R\sin\alpha}{\sqrt{\left(S-R\sin\alpha\right)^2 + \left(R\cos\alpha\right)^2}}\right] \tag{10}$$

Fig. 3(a) compares the φ calculated by the numerical model with the data from the article by Fan [26], and good agreement is obtained. As can be seen, the distribution of φ is symmetrical approximately. Fig. 3(b) shows the radiative heat flux distribution on the outer surface of the tube under a typical working condition ($q_{\max}$ is 134 kW/m^2), and the highest radiative heat flux is about 134 kW/m^2 at the top part of the tube, while the lowest one is located at the bottom, about 23.3 kW/m^2, due to the low heat reflected from the boiler furnace wall. Then, the non-uniform radiative heat flux boundary condition is used at the cooling wall tube's outer surface.

2.3 Governing equations and boundary conditions

2.3.1 Thermal-hydraulic calculation

A three-dimensional steady-state model containing continuity, momentum and energy equation is developed to study the heat transfer process. The details of the governing equations were described in previous study [27–29], thus, it is not presented here. Because of the high Reynolds number of sCO_2, the numerical model is assumed fully developed turbulent flow. The selection of turbulence models significantly contributes to the accuracy of the numerical results. Herein, three turbulence models, including the k-ω model [27], the SST model [28], and the k-ε model [29], are compared.

At the inlet, a fully-developed flow velocity (a parabolic velocity profile) is calculated as a function of average inlet velocity by a self-developed program. The inlet temperature (T_{in}) of 773 K and working pressure (P) of 30 MPa are adopted considering the actual working conditions in sCO_2 boilers [30]. The logarithmic wall function is employed [27] at the inner tube wall, and the outlet is set as the fully-developed assumption [31]. The thermophysical properties of sCO_2 as a function of temperature and pressure are obtained from the NIST REFPROP. The maximum residuals of all governing equations are set to be under 10^{-3} to ensure calculation convergence.

2.3.2 Simulations of the cooling wall

According to the operating conditions and data of the sCO_2 boiler, the T91 is used as the tube material, and Table 1 shows its physical properties. The inner wall surface under the turbulent flow model is solved using the thermal wall function.

A detailed structural analysis of the tube is essential to improve the safety and reliability of cooling wall and sCO_2 boiler. The thermal stress and mechanical stress are calculated in three directions which can be found in Ref. [32]. According to the von Mises theory [33], the equivalent stress (σ_{eq}) is defined as:

$$\sigma_{eq}=\sqrt{\frac{(\sigma_r-\sigma_\theta)^2+(\sigma_\theta-\sigma_z)^2+(\sigma_z-\sigma_r)^2}{2}} \quad (11)$$

To improve the accuracy of the simulation results, grid-independent analysis is also performed, and the relative error is less than 0.003.

2.4. Model validations

In order to verify the feasibility of the three turbulence models, the numerical simulations are controlled with the same working parameters in Table 2 as experiments [18]. As seen in Fig. 4, the numerical results on the fluid temperature show good agreement with the experimental data for all the turbulence models. The relative errors of the inner tube wall temperatures are within 8.84% of the SST model, 5.69% of the k-ω model, and 4.17% of the k-ε model, respectively. Thus, the k-ε model is selected in the latter simulations.

Because of the lack of experimental data in structural model calculations, the structural model is validated by

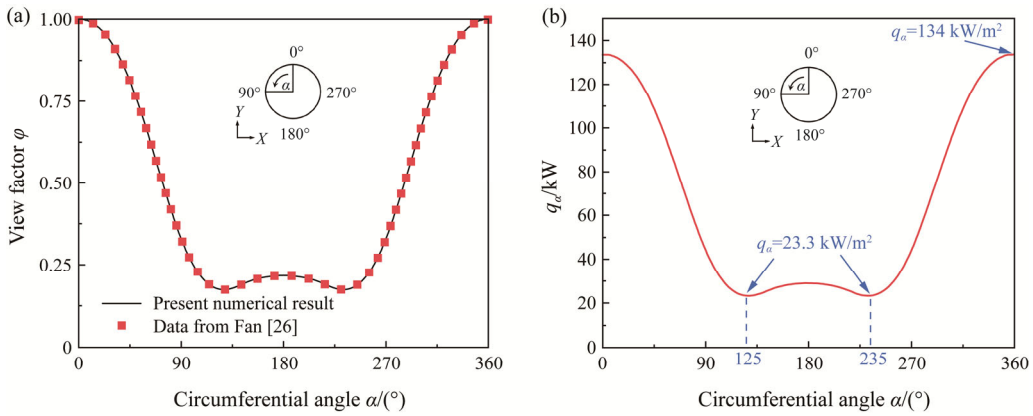

(a) Validation of φ against previous model (b) Radiative heat flux

Fig. 3 Circumferential distribution of φ and radiative heat flux

Table 1 Physical properties of T91

T/K	293	373	473	573	673	773	873	973
$\alpha/10^{-6}\cdot K^{-1}$	10.6	10.9	11.3	11.7	11.9	12.2	12.4	12.6
λ/W·(m·K)$^{-1}$	25.9	27.1	28	29.2	29.1	29	29.3	29
$E/10^3$ MPa	218	213	207	199	190	181	168	158
C_p/J·(kg·K)$^{-1}$	460	469	490	511	530	570	800	-
υ	0.29	0.3	0.3	0.3	0.29	0.3	0.32	0.35
ρ/kg·m^{-3}	7780							

Table 2 Representative experimental cases for validation

Parameter	G/kg·(m^2·s)$^{-1}$	L/m	T_{in}/K	q_w/kW·m^{-2}	P/MPa	d/mm	D/mm
Value	1002.4	2	394	250.22	15.672	10	12
Material	1Cr18Ni9Ti						

theoretical solutions [32]. The mechanical stress induced by applying pressure load of 30 MPa and thermal load resulted from 25 K temperature difference between the inner and outer surfaces are computed by the proposed numerical model and the theoretical method, respectively. As shown in Fig. 5, the mechanical and thermal stress curves obtained from the numerical calculations and the theoretical analysis are in good agreement, effectively validating the reliability of the structural model.

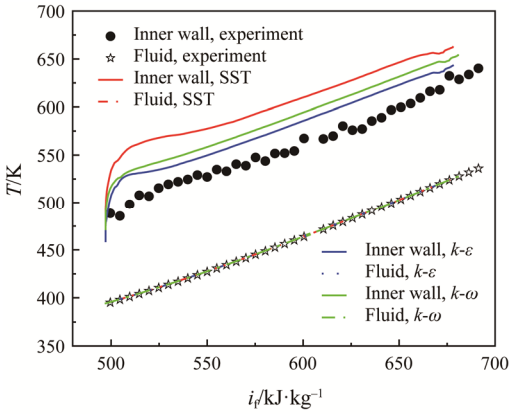

Fig. 4 Comparisons between simulation results and experimental data

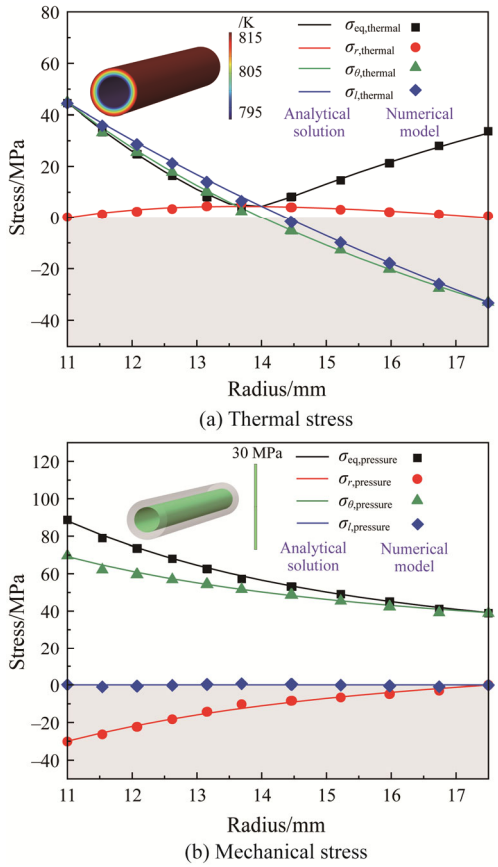

Fig. 5 Validation of structural model against theoretical solutions

3. Results and Discussion

3.1 Performance of traditional cooling wall tube

A three-dimensional numerical simulation of the conventional cooling wall tube (D of 35 mm and wall thickness of 6.5 mm) is investigated, and the simulation parameters are set as: the sCO_2 inlet mass flux (G) is 1800 kg/(m^2·s), the sCO_2 inlet temperature is 773 K; the working pressure is 30 MPa, and q_{max} is 240 kW/m^2 for the NUH case. As for the uniform heat flux (UH) case, the total heat flux is the same as the NUH case.

The temperature and stress profiles of the traditional cooling wall tube are shown in Fig. 6 and Fig. 7, respectively. For the UH case, the temperature and stress in the circumferential direction of the pipe wall are distributed axially symmetrically. The maximum stress is caused by a combination of thermal and pressure loads, and occurs in the inner tube wall region. In the NUH case, the equivalent stress and the thermal stress are much larger, especially at the fireside (α=0°). Compared Fig. 6(c) with Fig. 7(b), the stress distribution is proportional to the temperature difference of the outer wall ($\Delta T_{w,o}=|T_{w,o}-T_{ave}|$, in which T_{ave} is the cross-sectional average temperature), which agrees well with Ref. [26]. It can be concluded that the significant CTD induced by the NUH yields severe thermal stress. In addition, the thermal stress is far larger than the mechanical stress. Under the NUH conditions, the total stress also consists of two components. But the thermal stress dominates. Thus, effective methods or designs to reduce the thermal stress are necessarily needed in the subsequent study.

Fig. 8 illustrates the deformation of the cooling wall tube. It can be found that the cross-sectional displacements (x and y direction displacements) are proportional to the temperature difference for both the UH and NUH cases. The NUH has a prominent influence on the cross-sectional displacements, especially in the y-direction. The maximum y-direction displacements are about 0.12 mm and 1.5 mm under the UH and NUH cases, respectively. Therefore, the circumferential temperature gradient should be reduced.

3.2 A new cooling wall tube structure

An eccentric tube structure, as shown in Fig. 9, is proposed to optimize the traditional cooling wall tube. The outside surface of the tube is unchanged. The center of the inside tube surface is moved toward the fireside while the inside radius is unchanged. Thus, the tube thickness (which is proportional to conduction thermal resistance) distribution in the circumferential direction is changed. The wall thickness of the fireside decreases, and the wall thickness of the rear side increases. These modifications distribute the circumferential thermal

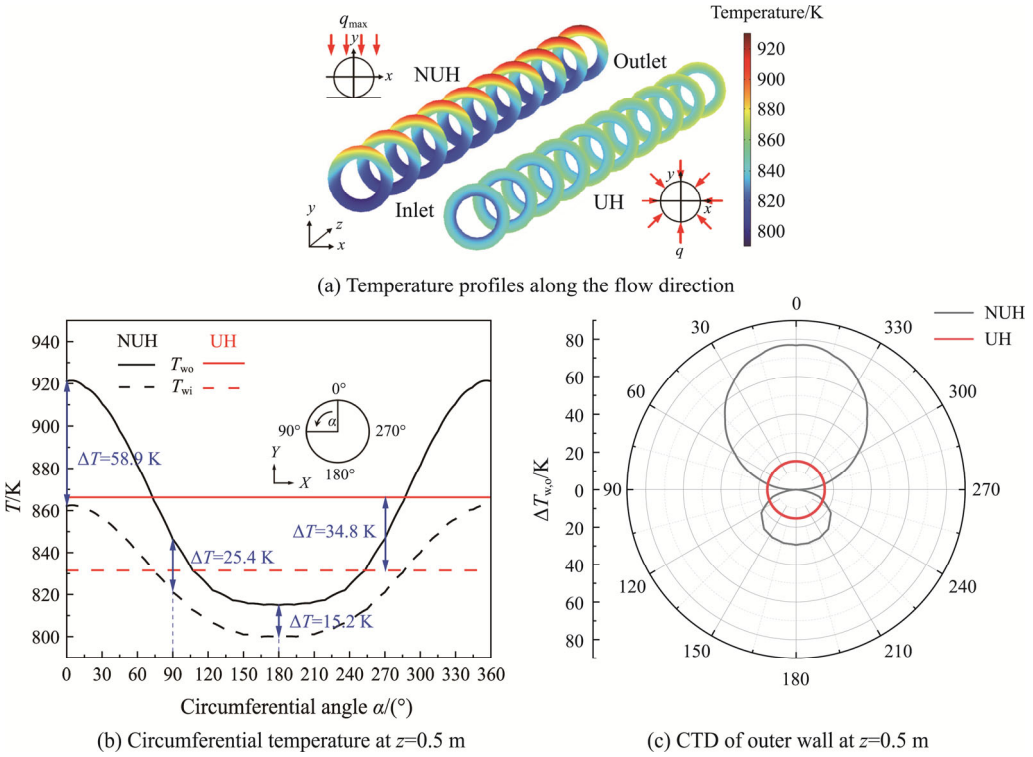

(a) Temperature profiles along the flow direction

(b) Circumferential temperature at z=0.5 m

(c) CTD of outer wall at z=0.5 m

Fig. 6 Temperature profiles of traditional cooling wall tube under UH and NUH cases

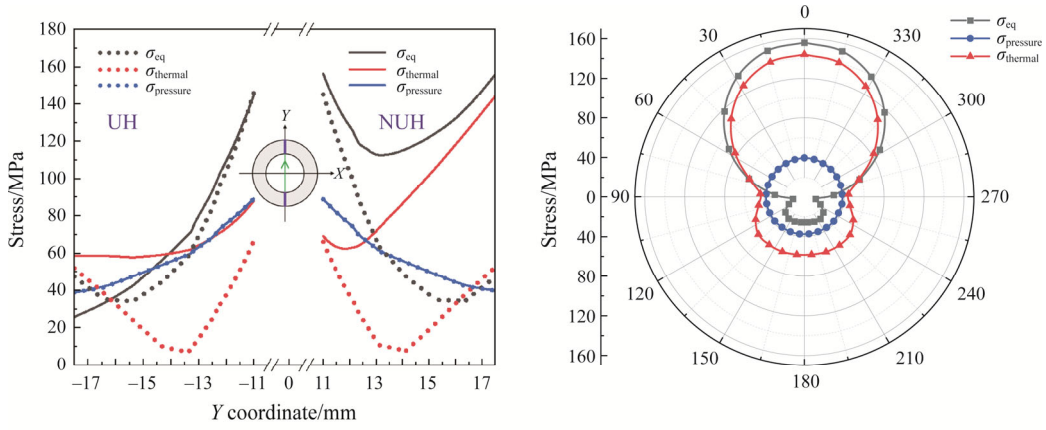

(a) In radial direction along y axis

(b) Outer tube wall under NUH

Fig. 7 Stress profiles of traditional cooling wall tube at z=0.5 m

resistance inversely to the heat flux distribution. The higher heat flux matches the smaller conduction thermal resistance.

Eccentricity (E_c) is employed to measure the uneven distribution of wall thickness of the eccentric tube, which is defined as:

$$E_c = \frac{e}{R-r} \tag{12}$$

where, e is the eccentric distance between the inner and outlet wall centers, and (R–r) is the initial tube wall thickness.

According to the definition of E_c, the wall thickness of the fireside decreases with the increase of E_c, leading to smaller conduction thermal resistance. The decrease of wall thickness at fireside is good for the heat transfer process. However, this may also cause safety problems when the wall thickness is too thin. Therefore, the minimum thickness of tubes under different working conditions is necessarily obtained, and it is calculated according to Ref. [34]

$$\delta_m = \frac{PD}{2\sigma_{as}\xi + 2PY} \tag{13}$$

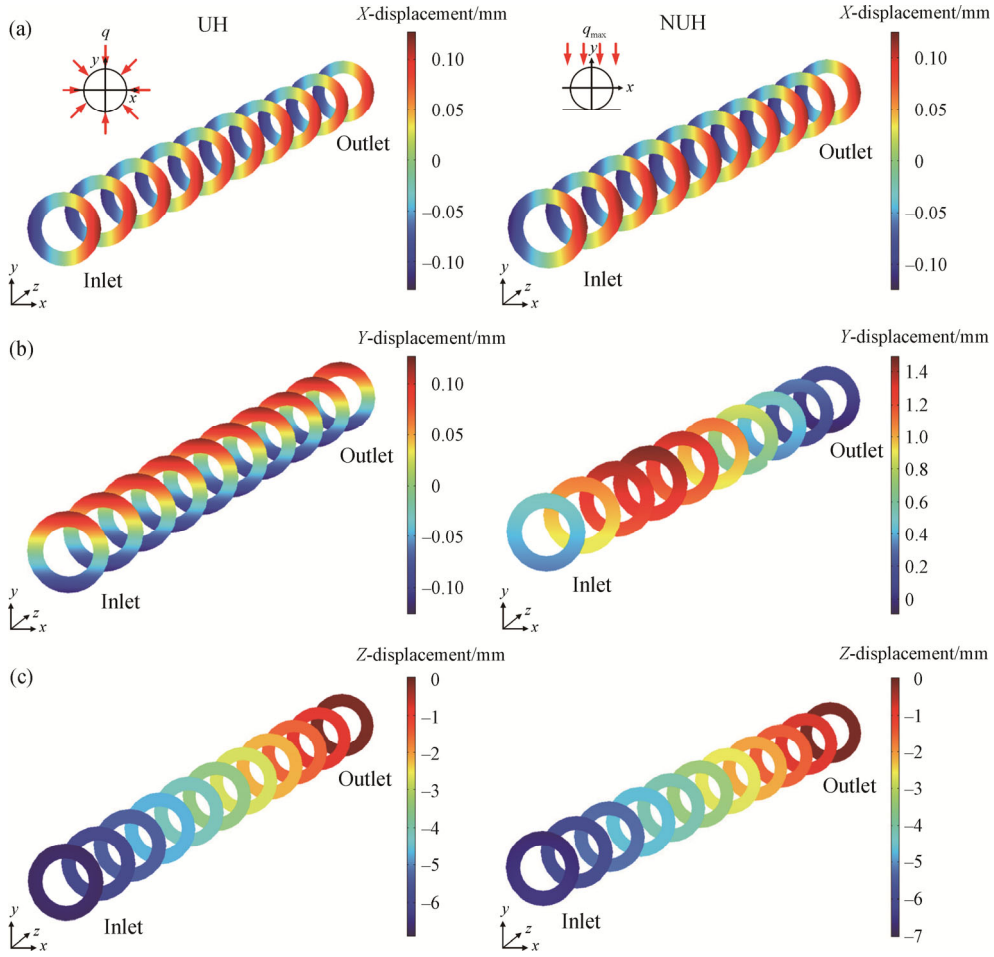

Fig. 8 Deformations of the cooling wall tube under UH and NUH cases

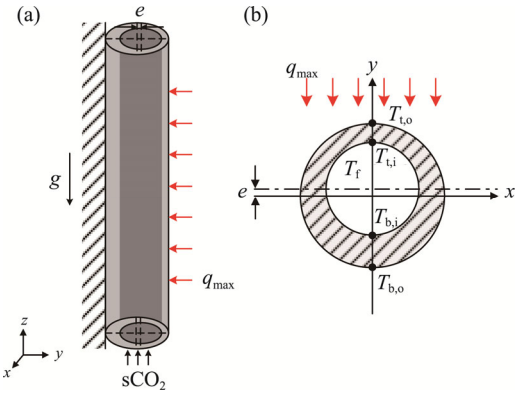

Fig. 9 Physical configuration of the eccentric cooling wall tube

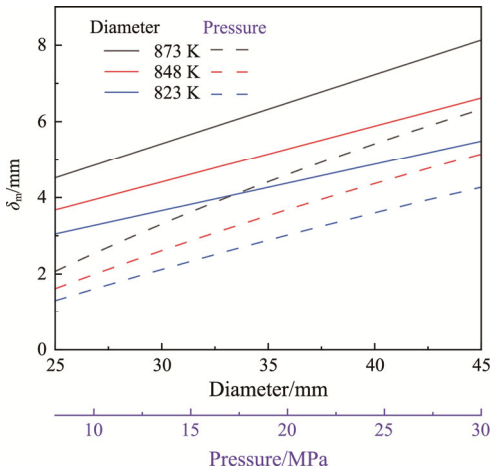

Fig. 10 δ_m as a function of temperature, pressure, and diameter

where δ_m is the minimum wall thickness, excluding the additional thickness caused by corrosion and wear; σ_{as} is the maximum allowable stress of the steel at working temperatures; ξ is the allowable stress correction factor, and Y is the correction coefficient. Fig. 10 displays δ_m with the change of internal pressure, isothermal tube temperature, and diameter for T91. As can be seen, δ_m increases with temperature, pressure, and diameter; thus, the value of E_c is set according to the working conditions.

3.3 Comparisons between the traditional and the eccentric cooling wall tube

According to the definition of E_c, the traditional cooling wall tube is an eccentric tube with E_c of 0. Five different eccentricities are selected as variables for numerical simulations to obtain the effects of E_c on the

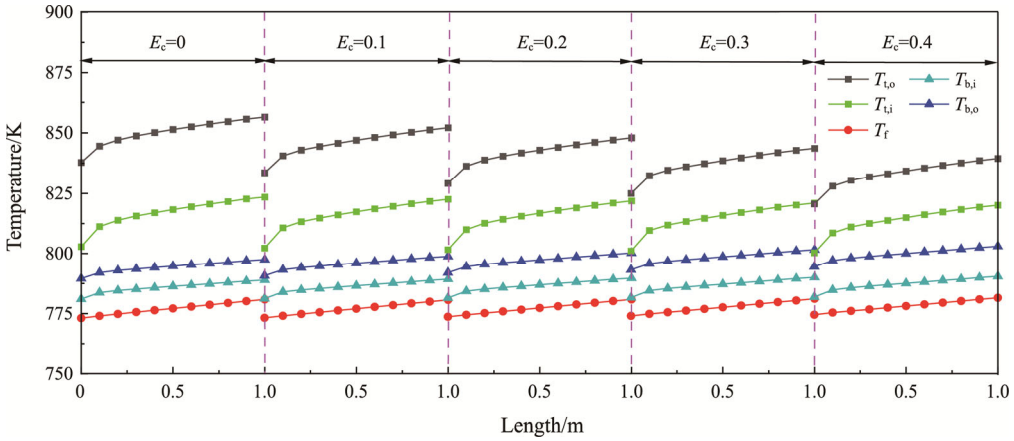

Fig. 11 Variations of cooling wall temperature with E_c

performances of the tube. The typical calculation conditions are defined for the sake of closeness to reality and ease of calculation as follows: the sCO_2 inlet mass flux, q_{max}, and the sCO_2 inlet temperature are 2000 kg/(m^2·s), 134 kW/m^2, and 773.15 K, respectively, and the working pressure is 30 MPa.

Fig. 11 shows the influences of E_c on the temperature distributions of the cooling wall. It is observed that the temperature difference between the inner and outer tube walls at the bottom generatrix is much smaller than that at the top generatrix because of the lower heat flux density at the bottom generatrix. As the actual circumferential heat flux of the tube is non-uniform, the maximum wall temperature at the top generatrix has a large impact on the tubes' safety. The outer wall temperature at the top generatrix ($T_{t,o}$) is effectively reduced by the eccentric tube structure. Furthermore, $T_{t,o}$ decreases with the increase of E_c. When E_c rises to 0.4, $T_{t,o}$ decreases by about 17 K compared with the traditional tube. The proposed eccentric tube structure effectively reduces the maximum temperature (T_{max}) of the tube.

It can be seen from Fig. 12 that the CTD is largely due to the circumferential NUH. Temperatures at the fireside are reduced effectively with the increase of E_c. The temperatures at the rear part increase slightly, which may be due to the enhanced heat transfer of sCO_2. Thus, the temperature difference is effectively reduced with the increase of E_c. The CTD decreases from 65.1 K to 46.8 K when E_c increases from 0 to 0.4. The CTD can be decreased by as much as 28.1% compared with the traditional tube at z=0.5 m. Meanwhile, it can be seen from Fig. 13 that the pressure drops of the tubes almost remain unchanged when the E_c changes.

Fig. 14 shows the comparison between the traditional and the eccentric tube when E_c is 0.4. The maximum thermal stress of the eccentric structure tube is reduced by about 26% due to the lower CTD, which agrees well

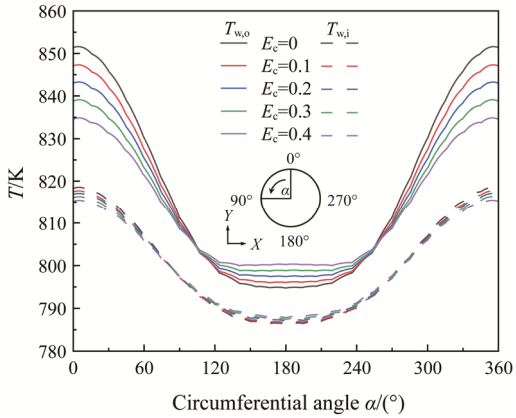

Fig. 12 Temperature profile of the cooling wall tube at z=0.5 m

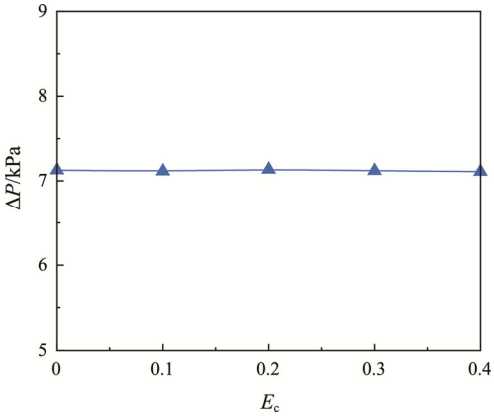

Fig. 13 Variations of the ΔP with E_c

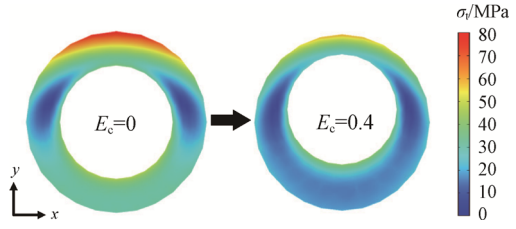

Fig. 14 Thermal stress profiles of traditional and the eccentric tube at z=0.5 m

with Ref. [26]. As the maximum thermal stress is almost proportional to the CTD, thus, only the variations of the CTD are investigated in the next section.

3.4 Effects of the tube material

Choosing a tube material requires not only considering the maximum temperature but also calculating the maximum stress generated by the temperature gradient and pressure together. The maximum allowable stress of metallic material is negatively related to temperature, so the higher pressure and temperature usually result in higher δ_m and poorer safety. Thus, the tube materials in sCO_2 boiler should accommodate the high temperature and pressure in addition to the cost. In this part, several common materials (T91, T92, 12Cr1MoVG, 15CrMoG, 1Cr18Ni9Ti, TP304H, Super304H, Sanicro25) are studied and compared.

Fig. 15 illustrates the variations of the minimum wall thickness δ_m with tube material at 25 MPa. δ_m changes with tube materials as the allowable stress is different for different materials. δ_m of Sanicro25 is the thinnest due to its large allowable stress, and it changes little with the temperature increase. Thus, Sanicro25 is a better material for cooling wall tube, while its cost is expensive. The properties of T91 and T92 are similar, and their costs are moderate. δ_m is thin at low temperatures, while it increases gradually with the temperature. Therefore, only a small E_c can be realized at high temperatures. The allowable stresses of 12Cr1MoVG and 15CrMoG change much with the increase in temperature, and their δ_m is too thick. Thus, they are not suitable for cooling wall tubes. E_c is also limited by δ_m, for example, the maximum E_c of TP304H and T92 is 0.22 and 0.43, respectively, under 25 MPa and 848 K.

The influences of E_c and tube material on the performance of cooling wall tube in typical working conditions as follows: the sCO_2 inlet mass flux, q_{max}, working pressure, and the sCO_2 inlet temperature are 2500 kg/(m^2·s), 25 MPa, 104 kW/m^2, and 773 K, respectively, are illustrated in Figs. 16–18.

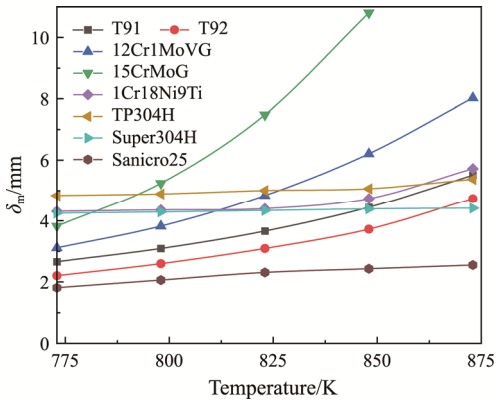

Fig. 15 δ_m as a function of tube material with an outer diameter of 35 mm

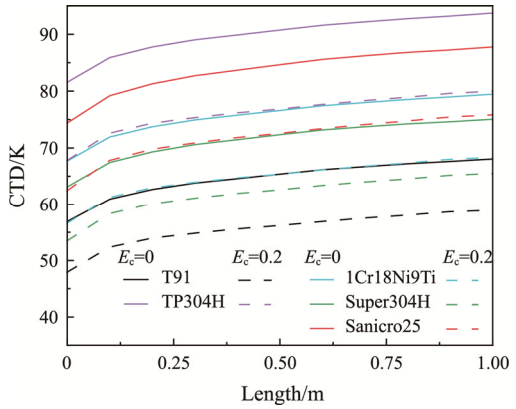

Fig. 16 CTDs as a function of E_c and tube material

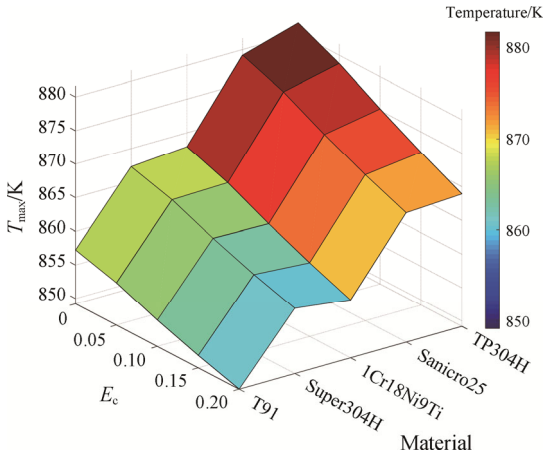

Fig. 17 T_{max} as a function of E_c and tube material

It can be observed from Fig. 16 that there exist big CTDs for all the cooling wall tubes due to the NUH, and the CTD increases continuously along the flow direction. The maximum CTDs occur at the outlet. It reaches 93.7 K for TP304H when the E_c is 0, while it is 68.1 K for T91. The CTDs are significantly reduced by the eccentric tube structure for all tubes. The CTD reduction reaches more than 10 K for TP304H, 1Cr18Ni9Ti, and Sanicro25 when the E_c increases from 0 to 0.2. Moreover, it reaches 14 K for TP304H.

Fig. 17 shows the influences of E_c and tube material on T_{max}. Tube material has great influence on T_{max}. T_{max} of T91 is the smallest, while it is the largest for TP304H. The maximum temperatures are significantly reduced by the proposed eccentric tube structure for all materials. T_{max} can be reduced by 8–13 K when E_c changes from 0 to 0.2.

It can be seen from Fig. 18 that variations of the maximum cross-sectional thermal stress ($\sigma_{t,max}$) are similar to the CTDs. $\sigma_{t,max}$ of T91 is the smallest while it is the largest for TP304H. When E_c is increased, $\sigma_{t,max}$ is significantly reduced for all the tube materials. Compared with the traditional tubes, $\sigma_{t,max}$ can be reduced by 10%–15% when E_c is 0.2.

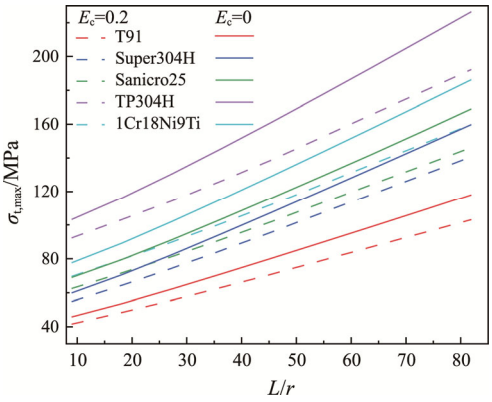

Fig. 18 $\sigma_{t,max}$ as a function of E_c and tube material

4. Conclusions

In this paper, a new cooling wall tube structure is proposed to enhance heat transfer and improve thermal-structural performance, and a thermal-hydraulic-structural coupling mathematical model is developed to investigate the new structure numerically. The conclusions are summarized below.

(1) A new cooling wall tube structure is proposed to match the non-uniform heat flux (NUH) with the circumferential thermal resistance of the tube by changing the eccentricity (E_c), which will facilitate to ensure the safety of the cooling wall tube. The new structure can effectively reduce the maximum temperature and circumferential temperature gradient. In contrast to the traditional cooling wall tube, the maximum temperature and circumferential temperature difference (CTD) of the new structure are reduced by 2% and 27.4% (16.8 K and 18.5 K), respectively, when the eccentricity increases from 0 to 0.4. Meanwhile, the pressure drop keeps almost the same as the traditional structure.

(2) A comparative analysis of the proposed structure and the conventional cooling wall tube structure is carried out. The performances with respect to operating parameters are numerically investigated. Both the maximum temperature and CTD decrease with the increase of E_c. When the E_c is 0.2, the maximum temperature of the new structure is decreased by 8–13 K; the CTD is reduced by 13%–15%, and the maximum thermal stress is reduced by about 10%–15% compared with the traditional structure under all the simulated working conditions, indicating that the new structure is superior to the traditional structure under NUH.

Acknowledgements

The authors appreciate the financial support provided by the National Natural Science Foundation of China (No. 52076075 and No. 52130608).

References

[1] Zhao S.F., Ge Z.H., Sun J., Ding Y.L., Yang Y.P., Comparative study of flexibility enhancement technologies for the coal-fired combined heat and power plant. Energy Conversion and Management, 2019, 184: 15–23.

[2] Gonzalez-Salazar M.A., Kirsten T., Prchlik L., Review of the operational flexibility and emissions of gas- and coal-fired power plants in a future with growing renewables. Renewable & Sustainable Energy Reviews, 2018, 82: 1497–1513.

[3] Ahn Y., Bae S.J., Kim M., Cho S.K., Baik S., Lee J.I., Cha J.E., Review of supercritical CO_2 power cycle technology and current status of research and development. Nuclear Engineering and Technology, 2015, 47(6): 647–661.

[4] Dostal V., A super critical carbon dioxide cycle for next generation nuclear reactors. Massachusetts Institute of Technology, 2004, 154(3): 265–282.

[5] Wang Y.J., Yu B.H., Gao S., Liu Q.B., Xu J.H., Performance analysis of cooling wall of supercritical CO_2 coal-fired plants. Journal of Thermal Science, 2022, 31: 1881–1890.

[6] Wang K., Zhang X., Zhang Z., Min C., Three-dimensional shape optimization of fins in a printed circuit recuperator using S-CO_2 as the heat-transfer fluid. International Journal of Heat and Mass Transfer, 2022, 192: 122910.

[7] Le Moullec Y., Conceptual study of a high efficiency coal-fired power plant with CO_2 capture using a supercritical CO_2 Brayton cycle. Energy, 2013, 49: 32–46.

[8] Maxson A., Booras G., Hume S., Miller J., Buckmaster D., Hogg D., Integration of indirect-fired supercritical CO_2 power cycles with coal-based heaters. The 6th International Supercritical CO_2 Power Cycles Symposium, Pennsylvania, USA, March 27–29, 2018.

[9] Xu J., Wang X., Sun E., Li M., Economic comparison between sCO_2 power cycle and water-steam Rankine cycle for coal-fired power generation system. Energy Conversion and Management, 2021, 238: 114150.

[10] Li X.L., Tang G.H., Fan Y.H., Yang D.L., A performance recovery coefficient for thermal-hydraulic evaluation of recuperator in supercritical carbon dioxide Brayton cycle. Energy Conversion and Management, 2022, 256: 115393.

[11] Fan Y.H., Tang G.H., Li X.L., Yang D.L., General and unique issues at multiple scales for supercritical carbon dioxide power system: A review on recent advances. Energy Conversion and Management, 2022, 268: 115993.

[12] Yang Y., Li H.Z., Zhang Y.F., Bai W.G., Yao M.Y., Coupled modeling of combustion and heat transfer

process of a supercritical CO_2 boiler. Fuel, 2020, 279: 118294.

[13] Xu J.L., Sun E.H., Li M.J., Liu H., Zhu B.G., Key issues and solution strategies for supercritical carbon dioxide coal fired power plant. Energy, 2018, 157: 227–246.

[14] Sun E.H., Xu J.L., Li M.J., Liu G.L., Zhu B.G., Connected-top-bottom-cycle to cascade utilize flue gas heat for supercritical carbon dioxide coal fired power plant. Energy Conversion and Management, 2018, 172: 138–154.

[15] Zhou J., Xiang J., Su S., Hu S., Wang Y., Xu K., Xu J., He L., Ling P., Zhu M., Key issues and practical design for cooling wall of supercritical carbon dioxide coal-fired boiler. Energy, 2019, 186: 115834.

[16] Wang J., Chen X., Zhang C., et al., Numerical investigation of heat transfer characteristics of supercritical CO_2 tube in combustion chamber of coal-fired boiler. Journal of Thermal Science, 2019, 28: 442–453.

[17] Li X.L., Li G.X., Tang G.H., Fan Y.H., Yang D.L., A generalized thermal deviation factor to evaluate the comprehensive stress of tubes under non-uniform heating. Energy, 2023, 263: 125710.

[18] Zhu B.G., Xu J.L., Wu X.M., Xie J., Li M.J., Supercritical "boiling" number, a new parameter to distinguish two regimes of carbon dioxide heat transfer in tubes. International Journal of Thermal Sciences, 2019, 136: 254–266.

[19] Li H.Z., Zhang Y.F., Yao M.Y., Yang Y., Han W.L., Bai W.G., Design assessment of a 5 MW fossil-fired supercritical CO_2 power cycle pilot loop. Energy, 2019, 174: 792–804.

[20] Zhou J., Zhu M., Xu K., et al., Key issues and innovative double-tangential circular boiler configurations for the 1000 MW coal-fired supercritical carbon dioxide power plant. Energy, 2020, 199: 117474.

[21] Liu C., Xu J., Li M., Wang Q., Liu G., The comprehensive solution to decrease cooling wall temperatures of sCO_2 boiler for coal fired power plant. Energy, 2022, 252: 124021.

[22] Munoz J., Abanades A., Analysis of internal helically finned tubes for parabolic trough design by CFD tools. Applied Energy, 2011, 88(11): 4139–4149.

[23] Li X.L., Tang G.H., Yang D.L., Fan Y.H., Xu J.L., Thermal-hydraulic-structural evaluation of S-CO_2 cooling wall tubes: A thermal stress evaluating criterion and optimization. International Journal of Thermal Sciences, 2021, 170(1): 107161.

[24] Duda P., Taler J., A new method for identification of thermal boundary conditions in water-wall tubes of boiler furnaces. International Journal of Heat & Mass Transfer 2009, 52(5–6): 1517–1524.

[25] Taler J., Duda P., Węglowski B., Zima W., Grądziel S., Sobota T., Taler D., Identification of local heat flux to membrane water-walls in steam boilers. Fuel, 2009, 88(2): 305–311.

[26] Fan Y.H., Tang G.H., Numerical investigation on heat transfer of supercritical carbon dioxide in a vertical tube under circumferentially non-uniform heating. Applied Thermal Engineering, 2018, 138: 354–364.

[27] Wang Y.J., Liu Q.B., Lei J., Jin H.G., Performance analysis of a parabolic trough solar collector with non-uniform solar flux conditions. International Journal of Heat & Mass Transfer, 2015, 82: 236–249.

[28] Menter F.R., Two-equation eddy-viscosity turbulence models for engineering applications. AIAA Journal 1994, 32(8): 1598–1605.

[29] Jones W.P., Launder B.E., The prediction of laminarization with a two-equation model of turbulence. International Journal of Heat & Mass Transfer, 1972, 15(2): 301–314.

[30] Fan Y.H., Tang G.H., Yang D.L., Li X.L., Wang S.Q., Integration of S-CO_2 Brayton cycle and coal-fired boiler: Thermal-hydraulic analysis and design. Energy Conversion and Management, 2020, 225: 113452.

[31] Vafai K., Chen J.L.S., Numerical heat transfer. ASME Publication, New York, 1989.

[32] Neises T.W., Wagner M.J., Gray A.K., Structural design considerations for tubular power tower receivers operating at 650°C. ASME International Conference on Energy Sustainability Collocated with the ASME International Conference on Fuel Cell Science, 2014.

[33] Wang K., Zhang Z.D., Zhang X.Y., Min C.H., Buoyancy effects on convective heat transfer of supercritical CO_2 and thermal stress in parabolic trough receivers under non-uniform solar flux distribution. International Journal of Heat and Mass Transfer, 2021, 175: 121130.

[34] Ortega J., Christian H., Clifford K., Structural analysis of a direct heated tubular solar receiver for supercritical CO_2 Brayton cycle. International Conference on ASME International Conference on Energy Sustainability Collocated with the ASME Power Conference, 2015.